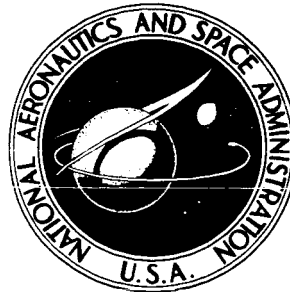


~~RESTRICTED DATA~~  
ATOMIC ENERGY ACT OF 1954

**NASA TECHNICAL  
MEMORANDUM**



UB  
NASA TM X-1445

UB  
NASA TM X-1445

**LIBRARY COPY**

OCT 4 1967

LEWIS LIBRARY, NASA  
CLEVELAND, OHIO

**EVALUATION OF PROCESSES  
FOR FABRICATING TUNGSTEN -  
URANIUM DIOXIDE  
HONEYCOMB CONFIGURATIONS**

NOV 09 2004

*by Paul F. Sikora and Charles P. Blankenship*

*Lewis Research Center*

*Cleveland, Ohio*

CLASSIFICATION CHANGED

To Unclassified

By authority of H. H. Marier

Date Jan. 3, 1973  
per lmd

EVALUATION OF PROCESSES FOR FABRICATING TUNGSTEN -  
URANIUM DIOXIDE HONEYCOMB CONFIGURATIONS

By Paul F. Sikora and Charles P. Blankenship

Lewis Research Center  
Cleveland, Ohio

**RESTRICTED DATA**

ATOMIC ENERGY ACT OF 1954

**GROUP 1**  
Excluded from automatic  
downgrading and declassification

[REDACTED] -TITLE UNCLASSIFIED  
This material contains information affecting the national defense of the United States within the meaning of the espionage laws, Title 18, U.S.C., Secs. 793 and 794, the transmission or revelation of which in any manner to an unauthorized person is prohibited by law.

**NOTICE**  
This document should not be returned after it has satisfied your requirements. It may be disposed of in accordance with your local security regulations or the appropriate provisions of the Industrial Security Manual for Safe-Guarding Classified Information.

NATIONAL AERONAUTICS AND SPACE ADMINISTRATION

[REDACTED]



# EVALUATION OF PROCESSES FOR FABRICATING TUNGSTEN - URANIUM DIOXIDE HONEYCOMB CONFIGURATIONS (U)

by Paul F. Sikora and Charles P. Blankenship

Lewis Research Center


## SUMMARY

Three methods of fabricating tungsten - uranium dioxide honeycomb fuel-element configurations have been developed under NASA sponsorship. These methods include hot isostatic compaction, hot pneumatic impaction, and green-state forming and sintering. All three processes were successful in consolidating tungsten-coated uranium dioxide particles in nearly fully dense dispersion-type composites of the desired honeycomb configuration.

Evaluation of the fabricated honeycomb grids indicated that the microstructure and overall integrity of the composites were generally good although occasionally microporosity and web cracking were encountered. This evaluation also indicated that the fuel loading in these grids could be varied radially from 30 volume percent uranium dioxide at the center to 10-volume percent at the periphery. The fuel loading variation was accomplished both in a continually varying gradient and in stepwise increments. Generally good control of the web thickness and channel dimensions was achieved, but substantial improvements in dimensional control are needed.

Evaluation of honeycomb grids and similarly produced plates at temperatures to 2500<sup>0</sup> C indicated that better control of the starting materials is necessary to improve the high-temperature performance of these composites. These high-temperature tests also demonstrated the need for unfueled tungsten claddings on all surfaces of the composites. The honeycomb grids exhibited good dimensional stability under thermal-cycling tests.

Although all the processes demonstrated the feasibility of producing tungsten - uranium dioxide honeycomb configurations, the hot isostatic compaction and hot pneumatic impaction processes appear more promising for use in fabricating actual fuel elements. However, further development of the processes is necessary before fuel elements can be produced.



## INTRODUCTION

Space propulsion by means of nuclear rockets is being investigated at the Lewis Research Center with particular emphasis on a tungsten-base thermal reactor termed the Tungsten Water-Moderated Reactor (TWMR) (refs. 1 and 2). The conceptual design of the TWMR utilizes conventional structural materials, hydrogen as the propellant, and dispersion-type fuel elements of uranium dioxide ( $\text{UO}_2$ ) particles in tungsten (W). The fuel elements require a high surface area to volume ratio for maximum heat transfer to the hydrogen propellant. Two of the possible configurations that meet this requirement are an array of concentric cylinders and the hexagonal-celled honeycomb shown in figure 1. Several of these short stages would be used to make up each reactor fuel element.

Two of the more serious materials problems encountered during a study of tungsten- $\text{UO}_2$  fuel composites have been the rapid loss of  $\text{UO}_2$  from the composites at conditions simulating reactor operation (exposure to hydrogen gas at temperatures to  $2500^\circ\text{C}$  for times up to 10 hr) and the fabrication of complex fuel-element geometries. Methods of reducing fuel loss in tungsten- $\text{UO}_2$  composites to tolerable levels for use in nuclear space power applications have been developed (ref. 3) and were incorporated in the fuel element fabrication studies described herein. These methods include precoating the  $\text{UO}_2$  particles with tungsten, stabilizing the  $\text{UO}_2$  with metal oxide additives, cladding the exposed surfaces with a thin layer of unfueled tungsten, or a combination of these. Most of the fabrication effort was directed toward fabricating the honeycomb geometry that was thought to be more difficult to fabricate but which appeared to offer greater mechanical stability than the concentric cylinders because of its greater rigidity (ref. 2). Therefore, three methods of producing these honeycomb grids were simultaneously investigated by different organizations under NASA-sponsored contracts:

- (1) Hot isostatic compaction (HIC), reference 4
- (2) Hot pneumatic impaction (HPI), reference 5
- (3) Green-state forming and sintering (GSF), reference 6

These studies were directed toward demonstrating process feasibility and toward developing the fabrication methods needed to attain the following design goals (as described in refs. 1 and 2):

- (1) Integrally sound (crack free) structure conforming to the configuration and dimensions shown in figure 2
- (2) Radial variation in fuel loading from 30 volume percent  $\text{UO}_2$  at the center of the grid to 10 volume percent at the periphery to even out the heat flux across the grid (fuel loading uniformity within each zone, shown in fig. 2, should be  $\pm 1$  volume percent  $\text{UO}_2$ )
- (3) Fully dense composites (greater than 98 percent of theoretical) to attain maximum strength in the matrix



- [REDACTED]
- (4) Process reproducibility as to dimensions, fuel distribution, structure (micro and macro), and mechanical strength
  - (5) Exclusion of foreign elements that might be deleterious to fuel retention properties

In addition to the fabrication of honeycomb grids by one process, each contractor was required to fabricate plate samples that would have structures representative of those in honeycombs fabricated by that process. These plate samples were used to determine the high-temperature mechanical properties and to evaluate the fuel retention capabilities of composites fabricated by each process.

This report summarizes and evaluates the results of the honeycomb fabrication studies and indicates the progress which was made toward attainment of the goals just given. Areas that require additional development efforts to meet the program goals also are described. Data are presented from evaluation studies made at Lewis of representative samples fabricated by each process. These samples were examined for integrity, density, chemical composition, dimensional tolerances, and fuel loading distribution. In addition, the high-temperature tensile strength of representative plate-type composites was determined, and the thermal behavior under simulated reactor operating conditions was characterized.

## FABRICATION PROCESSES

The processes for fabricating honeycomb-type, fuel-element configurations are summarized briefly in this section and are described in detail in the reference cited. In studying these processes, the feasibility of their use for fabricating this configuration was the primary objective. Once this objective was demonstrated, major emphasis was placed on further development of the processes to attain process reproducibility. However, the extent of these programs did not allow complete study and optimization of all processing parameters. Therefore, further study is required on all three processes to fully define the process limitations.

### Hot Isostatic Compaction

In the hot isostatic compaction process, inert gas at high pressure and temperature in an autoclave was used to consolidate component materials in a suitable container. Process variables and other details of this study are described in reference 4. Fabrication of honeycomb grids by this process required a rather complex container assembly with sacrificial molybdenum mandrels positioned in photoetched molybdenum templates to

CONFIDENTIAL  
[REDACTED]

[REDACTED]

produce the desired configuration that is shown in figure 2. As illustrated in figure 3, this assembly, after being placed in the molybdenum container, was loaded with the fueled material and vibratorily compacted. The hot pneumatic impaction process, also shown in figure 3, is discussed in the following section.

A radial variation in fuel loading was achieved by a "removable dam" technique. This technique consisted of separating the zones, outlined in figure 2, with barriers, loading each zone individually with  $\text{UO}_2$  particles coated with tungsten to obtain the desired fuel loading, and removing the barriers. The resultant fuel loading varied in 4 percent increments from 30 volume percent at the center to 10 volume percent at the periphery.

After evacuation and sealing, the assembly was placed in an autoclave and compacted by heating to about  $1650^\circ\text{C}$  under a pressure of 30 000 psi ( $207 \times 10^6 \text{ N/m}^2$ ) for 2 to 3 hours. After compaction, molybdenum components were removed by selective chemical dissolution in nitric acid. A high degree of bonding and densification was achieved under these conditions, and composite densities produced were greater than 99 percent of theoretical.

## Hot Pneumatic Impaction

The hot pneumatic impaction process is described in detail in reference 5 and is similar to that used for hot isostatic compaction, as illustrated in figure 3. In the pneumatic impaction process (a high-energy-rate, pneumatic-mechanical process), a honeycomb assembly of sacrificial mandrels was placed in a cylindrical impaction container. This assembly was loaded with tungsten-coated  $\text{UO}_2$  particles, vibratorily compacted, heated to the impaction temperature while under evacuation, and impacted in a closed-die assembly. Container and mandrel materials were removed by chemical dissolution. Tungsten- $\text{UO}_2$  honeycomb grids, conforming to figure 4 and having densities greater than 99 percent of theoretical, were fabricated by this process using molybdenum containers and mandrels, a temperature of  $1600^\circ\text{C}$  and an impaction pressure near 300 000 psi, ( $207 \times 10^7 \text{ N/m}^2$ ).

Two methods were used to obtain radial fuel loading: (1) a removable dam technique similar to that utilized in the hot isostatic compaction process and (2) a machine loading technique that yielded a linear rather than a stepped variation in fuel content. Tungsten-coated particles containing 10 and 30 volume percent  $\text{UO}_2$  were blended in the required proportions to achieve the desired fuel loading in the removable dam technique. In the machine loading technique, a mechanical feeding system, consisting of automated fixtures, proportioned the two fuel loadings into the mandrel assembly to obtain the desired linear variation in fuel loading.

[REDACTED]

Although there is a similarity between hot pneumatic impaction and hot isostatic compaction, consolidation is effected by totally different means. In the hot pneumatic impaction process, the mandrels are upset, expand outward, and cause the particles to bond and densify. In hot isostatic compaction, the entire assembly contracts radially inward with little, if any, deformation of the mandrels.

## Green-State Forming and Sintering

A green-state forming and sintering process, described in reference 6, used a special powder metallurgy technique (as shown in fig. 5) to fabricate honeycomb grids conforming to figure 2. A binder, a plasticizer, a solvent, and the tungsten-coated  $\text{UO}_2$  particles were blended into a plastic mass. Fines, unfueled tungsten particles, were added to the coated particles to enhance sintering. When the appropriate consistency was attained, the plastic mass was passed through a rubber-type mill to form a pliable green sheet. A fueled green sheet was clad with unfueled tungsten by sandwiching it between two unfueled tungsten green sheets, and the assembly was passed through the mill to ensure good bonding between the sheets. This laminated sheet then was passed through a corrugating mill and sized in a die. The nodes of the corrugation were ground to half their original thickness, and the ground surfaces were glued to surfaces of similarly prepared sections to form the hexagonal channels.

Radial variations in fuel loading were achieved by joining small corrugated segments of various fuel loadings to form  $60^\circ$  wedge-shaped sections. These wedges then were precision ground and joined to form the cylindrical honeycomb. These glued assemblies were dried and presintered to remove the binder, the plasticizer, and the solvent. Densities in excess of 98 percent of theoretical were obtained with this process by final sintering in hydrogen gas to  $2450^\circ \text{C}$  for 4 hours.

## SPECIMENS AND EVALUATION PROCEDURES

The governing contract in each fabrication study specified the number of specimens to be furnished. Unfortunately, specimens differed in some respect among the contractors because of economic factors, technical difficulties, and time schedule limitations. Details of the specimen variations and a brief description of the evaluation procedures are presented in the sections that follow.

~~CONFIDENTIAL~~

## Specimens Evaluated

The geometry, fuel loading distribution, and additive content of the honeycomb grids fabricated by the three processes were not identical. For example, the grid geometry shown in figure 2 was desired, but it was more expedient in the study of the HPI process to modify the geometry of the grid to extend the fueled material to the outer wrap and to fill the small peripheral channels as shown in figure 4. This change was permitted because we felt that feasibility could be demonstrated without the additional time that would be required to fabricate the basic configuration.

Since cladding of tungsten- $\text{UO}_2$  composites enhances fuel retention (refs. 3 and 7), it was desirable to have all surfaces (including the propellant flow channels) clad with a thin (approx. 0.001 in. (0.025 mm)) layer of unfueled tungsten. Although this cladding could probably be applied by tungsten-vapor-deposition techniques (refs. 8 and 9) after the honeycomb grids are completely fabricated, it would be desirable (from cladding integrity and fabrication cost considerations) to have the cladding applied as an integral part of the fabrication process. The feasibility of applying claddings to the flow channels as part of the fabrication process was demonstrated by the GSF process, and thus the channels of all grids produced by this process were clad. The feasibility of cladding the channels as an integral part of the HPI fabrication process was demonstrated in a preliminary study described in reference 5. The cladding was applied in this process by precoating the molybdenum mandrels with tungsten and allowing this coating to bond to the tungsten matrix of the core during impaction. Because of the similarity of the HPI and HIC processes, we thought that the HIC grids could also be clad by precoating the mandrels. However, the grids produced by these processes and submitted for evaluation were not clad because of economic considerations and time limitations.

Concurrent with these fabrication studies, methods of improving fuel retention characteristics of tungsten- $\text{UO}_2$  composites at high temperatures, particularly under thermal cycling conditions, were being studied (ref. 10). At the time the fabrication studies were being conducted, yttria ( $\text{Y}_2\text{O}_3$ ) solid-solution additions to  $\text{UO}_2$  showed the greatest promise in stabilizing the  $\text{UO}_2$  under thermal cycling conditions and thereby retarding fuel loss. It was further shown that precoating the  $\text{UO}_2$  particles with tungsten reduced fuel loss by precluding the possibility of exposed  $\text{UO}_2$  on the surfaces (ref. 3). Furthermore, the individually coated fuel particles cannot readily become interconnected, and fuel loss by vaporization was decreased. Therefore, the samples obtained from these fabrication studies were produced from  $\text{Y}_2\text{O}_3$ -stabilized fuel that had been precoated with tungsten. In addition to the fabrication of grids, each contractor was to furnish flat plate specimens, 1 by 6 by 0.020 inch (2.5 by 15.2 by 0.050 cm), so produced as to be representative of the grid fabrication process. Plates containing 10, 20, or 30 volume

[REDACTED]

percent yttria-stabilized  $\text{UO}_2$  were intended for use in high-temperature fuel retention or tensile tests.

A summary of the samples included in the Lewis evaluation study is presented in table I, and representative honeycomb grids fabricated by each of the three processes are shown in figure 6. The results of chemical analyses of representative plates from each process are presented in table II. In most cases, the  $\text{UO}_2$  fuel loading was lower than the nominal desired values, and the halide contamination generally was excessive. Although the supplier's analyses of the  $\text{UO}_2$  substrate and the coated particle appeared to be in the desired range, it was subsequently found that the analytical techniques used for determining the halide content were not adequate (ref. 11). For example, reported fluorine analyses were probably lower than actual values because the total fluorine was not extracted during the analytical procedure. As of the present time, this problem has not been fully resolved, but the halide impurity levels reported in table II are thought to represent at least minimum values for the halide contents of the specimens.

## Evaluation Procedure

Grids and plates typical of each process were characterized on the basis of the following tests:

- (1) Nondestructive tests
- (2) Metallography
- (3) Density determinations
- (4) Fuel loading
- (5) Dimensional measurements
- (6) Thermal tests (to evaluate fuel loss)
- (7) Tensile tests

The procedures used in the above tests are described in the sections that follow.

Nondestructive tests. - Some of the honeycomb grids were subjected to ultrasonic and eddy current tests as described in reference 12. The prime purpose of these tests was to determine the integrity (i. e. , presence of cracks or other defects) of the interconnecting webs and outer wrap. These techniques utilized miniaturized probes that could be inserted into each of the channels.

Metallography. - Cross sections of plates and grids were examined in the as-fabricated condition and after thermal testing. Metallographic preparation consisted of mounting electrodischarge-machined sections of composites in epoxy, grinding the cut surface through 600-grit silicon carbide papers using water as the lubricant, and vibratory polishing with 0.3-micron alumina on nylon cloths for rough polishing and with 0.1-micron alumina on deep nap cloth for fine polishing. In most instances, the samples

[REDACTED]

were examined in the unetched condition only; however, a few samples also were examined after etching with Murakami's reagent.

Density determinations. - Densities of plate samples were determined on representative samples fabricated by each of the processes. The water displacement technique was used. On the basis of the chemical analysis for major constituents, these values were corrected to a percentage of the calculated theoretical density. Direct measurement of the density of grids was not attempted because of the complexity of the geometry and the variable fuel loading. Therefore, determination of the density of grids was dependent on metallographic examination.

Fuel loading. - Fuel loadings in the honeycomb grids were determined by analysis of autoradiographic films and by particle analysis from photomicrographs of grid sections. The autoradiographic images were obtained by placing grids on the surface of type AA X-ray film and holding for 20 hours. After development of the films, the resultant images were analyzed by measuring their relative density on a light-transmission densitometer. Included on the films were four reference images of tungsten- $\text{UO}_2$  plates containing 10, 20, 30, or 35 volume percent  $\text{UO}_2$  loadings to be used as a comparison basis for determining the radial fuel loading of the grid.

Photomicrographs of web sections also were used to measure fuel loading. Point count results were evaluated to determine their correlative factor with volume fraction.

Dimensional measurements. - The outside diameters and heights of representative grids were measured with a micrometer caliper. Web thicknesses were determined by means of a channel-probing instrument developed specifically for this purpose. This instrument (described in ref. 12) consists of a dial gage attached to two parallel, spring-loaded probes that are capable of penetrating the hexagonal holes of a honeycomb grid. The thickness of the web and any variations in thickness are indicated on the dial gage.

Thermal tests. - Two thermal tests were used in this evaluation study. One of these tests was a static thermal test that consisted of a single cycle of rapidly heating the sample in hydrogen gas to  $2500^\circ\text{C}$ , holding for 2 hours, and then rapidly cooling to room temperature. The other thermal test, a fast thermal-cycle test, consisted of rapidly heating the sample ( $<2$  min) to  $2500^\circ\text{C}$  in flowing hydrogen gas at 35 standard cubic feet per hour ( $1\text{ s m}^3/\text{hr}$ ), holding for 10 minutes, and then rapidly cooling to room temperature ( $<2$  min). After every 5 or 10 cycles, the weight loss was measured; for purposes of this study, it was assumed that the change in weight was caused entirely by loss of  $\text{UO}_2$  from the composite. Both plates and grids were subjected to the cyclic thermal test; only plates were subjected to the static thermal test.

As previously discussed, encapsulation of the tungsten- $\text{UO}_2$  composites has been shown to aid fuel retention. Therefore, some plates were totally encapsulated with tungsten cladding, approximately 0.0005 inch (0.013 mm) in thickness, prior to thermal cyclic and static testing. This unfueled tungsten cladding was applied by vapor deposi-

[REDACTED]

tion from the hydrogen reduction of tungsten hexafluoride ( $WF_6$ ) (ref. 8).

Tensile tests. - Tensile specimens with a 1/4-inch (0.63 cm) reduced test section were electrodischarge machined from plates and were tested in a vacuum of  $10^{-5}$  torr ( $10^{-3}$  N/m<sup>2</sup>) at 2500° C at a cross-head speed of 0.03 inch (0.08 cm) per minute in accordance with the procedure outlined in reference 13. Specimens, containing 10, 20, or 30 volume percent  $UO_2$ , were tested. In addition to these tests, a series of tests from 1650° to 2500° C was made on HIC specimens containing 20 volume percent  $UO_2$ .

## RESULTS AND DISCUSSION

In view of the many differences (e. g., configuration, chemistry, etc.) existing in the samples received for evaluation, each process is treated individually in this discussion, and primary emphasis is placed on demonstrating the feasibility of producing a honeycomb grid configuration. In addition, areas that require additional development effort are delineated, whenever possible.

### Examination of As-Fabricated Samples

Integrity. - The results of the nondestructive tests indicate that some honeycomb grids were sound but that cracks in the webs and outer wrap existed in others. Seven grids were subjected to both ultrasonic and eddy-current tests for determining soundness; the results are listed in table III. Generally, the results indicate the presence of a few cracks in some of the grids produced by the HIC and HPI processes, but the one GSF produced grid that was inspected was crack free. Unfortunately, other grids produced by the GSF process were not inspected, and thus the reproducibility of the good quality of this grid was not determined.

Metallographic examination of some grids generally verified the inspection results. Defects were observed in the grids in which the nondestructive-test results indicated cracks, and no defects were found in the grids that were reported to be sound.

An example of a representative sound area of a HIC grid is shown in figure 7(a). Grids produced by this process tended to crack in the unfueled outer wrap, as shown in figure 7(b), and some cracking occurred in the webs of the honeycomb. Several factors could be responsible for this cracking. For example, the difference in thermal expansivity between the fueled core and the unfueled outer wrap could induce a severe stress in the outer wrap that is relieved by cracking after removal of the molybdenum can and mandrels. Cracking also could be induced by grinding during the cleanup of the grid after decanning.

[REDACTED]

A typical sound area of an HPI grid is shown in figure 8(a). Although the nondestructive-test results indicated some cracks existed in these grids, metallographic examination showed that the defects were more related to poor interparticle bonding and/or low preimpaction density which resulted in porosity such as that shown in figure 8(b).

A representative sound area of a grid produced by GSF is shown in figure 9(a). The cladding applied to the surfaces of the channels by this process is clearly evident. In addition, the somewhat uneven fuel distribution is indicated by the irregular pattern of the gray-colored fuel particles. (The black spots in the webs are caused by pullout of particles during metallographic polishing.) Although the one GSF-produced grid that was nondestructively inspected was sound, metallographic examination of other GSF grids indicated a lack of integrity due to poor bonding of segments in the fabrication process. A typical example of failure at glue joints and web intersections is shown in figure 9(b).

On the basis of metallographic examination, the tungsten matrix of the grids appeared to be dense in most areas. However, in other areas there did not appear to be sufficient interparticle bonding for a sound structure. This deficiency is probably related to the contaminants present in the coated particles rather than to the effect of processing. For example, figure 10 shows the highly densified structures that are possible by both the HIC and HPI processes when the composites are made from good starting materials. The samples shown in figure 10 were made from tungsten-coated particles of unstabilized  $\text{UO}_2$  and were relatively free of halide contamination (<50 ppm).

Observations of plate specimens revealed similar structures and were corroborated by the density determinations. The results of density determinations on plates fabricated by the three processes are presented in table IV. These results indicate that the goal of 98 percent minimum density was not attained in the plates. Considerable density variation occurred not only from plate to plate, but, in some cases, within a single plate. Some of this variation is probably caused by processing variables such as temperature gradients, precompaction density differences, and perhaps variations in time at temperature. In the case of the plates fabricated by HIC and HPI, it is believed that the low density (82 to 85 percent of theoretical density) of the  $\text{UO}_2$  particles used to produce these samples contributed to the density variation exhibited by these plates. However, the HPI plates have a higher average density and less variation than the other groups of plates.

Although problem areas exist with the integrity of grids produced by any of the three fabrication processes, we believe that sound honeycomb grids can be made by these processes providing improvements are made in control of the starting materials and fabrication parameters.

Dimensional measurements. - Results from dimensional measurements of webs from grids having the best dimensional tolerances are shown in figure 11. These grids



CONFIDENTIAL

represent the current status of the capability of each process to maintain dimensional control. On the basis of the program goal of  $\pm 0.001$  inch (0.025 mm) variation in web thickness from a nominal dimension of 0.020 inch (0.5 mm), it can be seen that 70 percent of the webs of HIC grids met the goal and that 65 percent of the webs of HPI grids and 53 percent of the webs of GSF grids were within the goal.

Most of the difficulties in maintaining close tolerances in the grids produced by the HIC or HPI processes stemmed from such factors as nonuniform mandrel movement, difference in compaction characteristics due to the density variations of the fuel particles and the variable fuel loading, and lack of complete optimization of process parameters (i. e., mandrel tolerances, die-can clearances, etc). In the case of the GSF grids, the broad range of web thicknesses points out the need for improved control of glue joints and glue-joint preparation, since nearly 50 percent of the webs were outside the specified tolerances.

Fuel distribution. - From a comparison of the microstructures shown in figures 7 to 9, it is evident that the fuel distribution is more uniform in the grids produced by either the HIC or the HPI processes. This results from the fact that all the tungsten matrix in composites produced by these processes is added as a coating on the fuel particles, while in the GSF process additional fine tungsten powder must be added to the coated particles to aid sintering.

Variations in fuel loading, radially from the center to the periphery, were relatively linear but not necessarily within the goal of  $\pm 1$  volume percent  $\text{UO}_2$ . The results of two methods for determining fuel loading, autoradiography and point count from metallographic prints, are plotted against relative location in the grid in figure 12. Although variations from the desired fuel loading are indicated, the linearity of the fuel loadings in grids representative of the three processes indicates that the different techniques for accomplishing the radially variable loading are good and may need only minor adjustments or refinements to be completely successful.

It should be noted that the techniques for determining fuel loading yield results that are relative to the standards used, particularly with the autoradiographic method. Since the standards used may not be completely applicable to these different types of specimens and may account for some of the deviations shown in the figure, the fuel loading values shown in figure 12 should not be considered absolute values. Also, it is not possible, at the current state of technology, to determine nondestructively if the fuel distribution meets the tolerance goal of  $\pm 1$  volume percent  $\text{UO}_2$ . Therefore, improvement of inspection techniques is required for use of composites such as these.

Part of the difficulty in attaining accurate fuel loadings in tungsten- $\text{UO}_2$  composites produced from tungsten-coated  $\text{UO}_2$  particles stems from the variations in  $\text{UO}_2$  particle size and tungsten-coating thickness in the coated particles. This problem is discussed in the appendix.

CONFIDENTIAL

## Thermal Behavior of Samples

Fuel loss tests. - Plate samples fabricated by each of the three processes were subjected to a 2-hour static test at  $2500^{\circ}\text{C}$  in a hydrogen atmosphere both in the as-fabricated condition and after total cladding (0.0005-in. - (0.013 mm) thick tungsten) by vapor deposition. From the results shown in figure 13, it can be seen that the fuel losses from the as-fabricated composites produced by HIC or HPI were high ( $>1$  percent), whereas the losses from two of the three types of composites (three different fuel loadings) produced by the GSF process were less than 1 percent. This difference probably results from the fact that the GSF samples, in the as-fabricated condition, have a tungsten surface clad approximately 0.001 inch (0.02 mm) thick, whereas no such intentional surface clads are present for the HIC and HPI plates. Apparently, the surface cladding on the GSF samples was effective in reducing fuel loss by vaporization. The GSF sample with 30 volume percent loading showed slightly higher fuel losses than either the HIC or HPI samples. The high degree of porosity and resultant low density (92 percent of theoretical) of this GSF specimen appeared to be responsible for its rapid rate of fuel loss. In addition, it was noted during a post-test metallographic examination of the 30 volume percent GSF sample that the grain size was considerably larger than was normally found in the GSF samples. The larger grain size is probably also responsible to some extent for the higher fuel loss of this sample.

The loss from the totally clad samples (with one exception) was much lower than those from the as-fabricated samples with most of the clad samples losing less than 1 percent of the  $\text{UO}_2$ . The one exception occurred in the HIC plates loaded with 10 volume percent  $\text{UO}_2$ , wherein the fuel loss was the same in both the as-fabricated and clad condition. Subsequent metallographic examination showed the cladding on this specimen to be defective and consequently to have afforded no protection to the sample. These data emphasize both the importance of obtaining a sound integral cladding on the samples and the protection afforded by the cladding even on composites produced from relatively poor starting materials.

Some examples of microstructures resulting from the relatively poor starting materials used in producing some of the specimens are shown in figure 14. The effect of the high fluorine content of the HIC samples resulted in a second phase (probably uranium tetrafluoride or a U-Y-F compound) surrounding some of the fuel particles (figs. 14(a) and (b)). Additionally, it can be seen that the  $\text{UO}_2$  particles were porous. The high chlorine content of the HPI samples after heating to  $2500^{\circ}\text{C}$  resulted in the beaded structure in the grain boundaries in figure 14(c) and is probably responsible for the porous section of a grid shown in figures 9(b) and 14(d). These grain boundary contaminants (thought to be tungsten oxychlorides) appeared to pin some of the matrix grain boundaries at the original particle interfaces and to outline the original interfaces be-

[REDACTED]

tween some of the tungsten-coated  $\text{UO}_2$  particles. A high degree of porosity in both the unfueled cladding and the fueled matrix existed in the GSF samples, as shown in figures 14(e) and (f). The porosity in the cladding of the plate sample (fig. 14(e)), however, is less than that in the grid sample (fig. 14(f)). The cause of this porosity is not known, but it does not appear to be directly related to the highly carbonaceous binder and plasticizer used. Chemical analyses showed the carbon content of this grid to be less than 10 ppm.

Additional thermal tests, consisting of rapidly heating the samples to  $2500^\circ\text{C}$ , holding for 10 minutes, rapidly cooling to ambient temperatures, and repeating the cycle for any desired number of cycles, were performed on as-fabricated plates and grids from each process. In figure 15 fuel loss is plotted against the number of thermal cycles. The results shown are for plates containing 20 volume percent  $\text{UO}_2$  and for grids that also average about 20 volume percent  $\text{UO}_2$ . There does not appear to be any appreciable difference in fuel loss among the grids up to 30 cycles. A larger difference in fuel loss was observed after 50 cycles, but these differences are not thought to be significant at these relatively high loss levels.

In general, fuel losses from plates were higher than those from grids, except in the case of the GSF material. The lower losses from the GSF material are probably a result of the unfueled tungsten cladding on the major surfaces and the much lower halide content of these samples. Metallographic examination of the GSF grids and plates after testing showed that the difference in behavior of the GSF plates and grids is probably caused by differences in quality of the unfueled tungsten cladding. The claddings were integrally sound on the plates, whereas considerable porosity was evident in the cladding of the grid channels. The GSF plate samples with good quality claddings on the major surfaces retained the fuel relatively well (<5 percent fuel loss after 50 cycles). We believe that the excessive fuel loss (>1 percent) from the grids and plates during thermal cycling is most likely related to the lack of complete cladding and to the starting material problems discussed earlier. There does not appear to be any indication, particularly in the HIC and HPI grids, that fabrication procedures are related to the high fuel losses.

The thermal cyclic test appears to be more severe for plate samples than for grid samples. This difference is probably related to the greater surface-to-volume ratio of plates as compared with grids. Thus the methods developed to reduce thermal cyclic fuel losses in plate-type tungsten- $\text{UO}_2$  composites (ref. 3) should be at least as effective in reducing fuel losses from honeycomb grids.

One of the most important results of the thermal cyclic tests is that none of the honeycomb grids, even after 50 thermal cycles, showed any evidence of distortion, warpage, or gross changes in length or diameter. This result is an indication of the good mechanical stability of honeycomb grids under these conditions.

[REDACTED]

Tensile tests. - The ultimate tensile strength of one group of HIC plates containing 20 volume percent  $\text{UO}_2$  was determined over the temperature range  $1650^\circ$  to  $2500^\circ$  C, and the results are plotted in figure 16. For comparison, a curve of tensile strength against temperature for a group of plates fabricated by hot roll compaction of tungsten-coated  $\text{UO}_2$  particles (as fabricated by the method described in ref. 11) is also included in figure 16. In both cases, the strength decreases with increasing temperature; however, the strength of the roll compacted material is considerably higher than that of the HIC material at temperatures up to at least  $2500^\circ$  C. This result is probably related to the difference in density; the roll compacted plates had a density greater than 99 percent of theoretical compared with about 95 percent for the HIC plates tested. Another contributing factor could be the difference in halide contamination (about 5600 ppm fluorine for HIC plates against about 400 ppm fluorine for the roll compacted plates), since halide contaminants are believed to cause internal generation of porosity under these test conditions (ref. 11). Also a third factor, in combination with those discussed previously, could be the strengthening of tungsten- $\text{UO}_2$  composites that results from mechanical working and partial elongation of the  $\text{UO}_2$  particles during roll compaction (ref. 14).

Additional tensile tests at  $2500^\circ$  C were conducted on plates fabricated by all three processes and with various fuel loadings. The results of these tests listed in table V are averaged values of two tests for each material. The observed strength differences are believed to be caused primarily by microstructural differences such as the type and amount of microporosity, the tungsten grain size, and the extent of deformation of the  $\text{UO}_2$  particles.

The finely dispersed matrix porosity is much higher in the GSF plates than in either the HIC or HPI plates. This porosity appears as tiny specks in the tungsten grains and probably stems from different sources. In the GSF samples, the porosity appears to be related to the process since it is present in the as-fabricated samples, shown in figure 17(d), whereas, the fine matrix porosity present in both the HIC and HPI as-tested samples is not present in the as-fabricated samples. In the latter cases, the porosity is probably caused by the halide contamination (ref. 7).

There is also a wide range of grain size in the tungsten matrices of these specimens. For example, in figure 17 the HIC plates show a large grain size, the GSF plates show a fine grain size, and the HPI plates show an intermediate grain size, much closer to that of the HIC specimens.

The mode of fracture in the tensile tests was different for the various materials (as shown in fig. 17). In the case of the HIC samples, it was found that the fracture occurred intergranularly with some evidence of ductility. However, both the HPI and GSF specimens fractured in a brittle manner. The difference in mode of fracture between the HIC and HPI specimens is most likely related to the grain size of the tungsten matrix. The HIC samples show a large grain size and some ductility, whereas the HPI and

~~CONFIDENTIAL~~

GSF samples have smaller grain size and little or no ductility. The finer grain structure in the HPI and GSF samples is most likely related to the contamination present in the particles. It is thought that this contamination inhibited growth of the tungsten grains in the HPI-produced composites. Since both the HIC and HPI processes have similar thermal histories, the resultant grain sizes should be equivalent.

## ADDITIONAL PROCESS DEVELOPMENT

The principal areas that need additional development effort for some or all of the processes are the following:

(1) Better dimensional control must be attained. In the hot isostatic compaction and hot pneumatic impaction processes, this control can probably be achieved by improvements in mandrel support during fabrication, better control of mandrel dimensions and straightness, and/or optimization of process variables.

(2) Improved control of fuel loading must be accomplished. This can probably be achieved by using starting materials that are closer to the desired loading and by minor refinements in the methods of distributing the fueled particles.

(3) Methods for cladding all exposed surfaces of honeycomb grids must be developed to improve fuel retention at elevated temperatures. This improvement can probably be achieved by mandrel coating techniques or by subsequent vapor-deposition coating techniques.

## Appraisal of Process Capabilities

During the course of the three process development programs and during this evaluation study, some advantages and disadvantages of each process became apparent. Some of these pertain to the TWMR honeycomb grid, while others pertain to other types of tungsten- $\text{UO}_2$  fuel elements.

The advantages and disadvantages of each process are as follows:

Advantages of hot isostatic compaction:

(1) Dimensions, especially flat to flat, should be good since the mandrels do not deform.

(2) Grids containing high fuel loadings ( $>50$  vol. %) can be compacted.

(3) Batch compaction is possible but requires larger equipment.

(4) Grid lengths up to about 12 inches may be possible, if required, but larger equipment would be necessary.

Advantages of hot pneumatic impaction:

~~CONFIDENTIAL~~

[REDACTED]

(1) More complex geometries of a heterogeneous cross section can be more easily produced than by the other two processes.

(2) Grids containing high fuel loading (>50 vol. %) can be compacted.

(3) The process is amenable to mass production.

Advantages of green-state forming and sintering:

(1) Surface cladding of flow channels can be easily accomplished.

(2) The process is amenable to mass production.

(3) Complex geometries and shapes are possible.

(4) Lengths in excess of 12 inches are possible.

Disadvantage of hot isostatic compaction: It may be more difficult to fabricate fuel element configurations with heterogeneous cross sections.

Disadvantages of hot pneumatic impaction:

(1) Most limited in length (L/D, 2 to 2.5:1).

(2) Dimensional control may not be as good as with hot isostatic compaction since deformation of mandrels is required.

Disadvantages of green-state forming and sintering:

(1) Dimensional control may be more difficult than with other processes since mandrels are not used during sintering.

(2) Glue joints are potential weaknesses.

(3) Fuel loading probably cannot exceed about 45 volume percent.

(4) Temperature control during processing is much more critical than for other processes.

(5) Reproducibility probably would be more difficult to attain.

Based on these factors and the results presented in this report, we believe the hot isostatic compaction and hot pneumatic impaction processes hold the most promise for use in fabricating tungsten- $\text{UO}_2$  fuel elements for nuclear rocket reactors.

## CONCLUSIONS

Processes for fabricating tungsten - uranium dioxide honeycomb configurations were studied and the following conclusions were reached:

1. The feasibility of fabricating complex geometries, such as honeycomb grids, has been established for three processes: hot isostatic compaction, hot pneumatic impaction, and green-state forming and sintering. The former two processes appear to be more promising for producing tungsten - uranium dioxide ( $\text{UO}_2$ ) fuel elements for nuclear rocket reactors.

~~CONFIDENTIAL~~

2. All three processes demonstrated the capability of using tungsten-coated particle of  $\text{UO}_2$  containing metal oxide stabilizers.
3. Necessary radial variations in fuel loading were demonstrated by all three processes.
4. Good starting materials are essential for good fuel retention, fuel distribution, and dimensional control.
5. Honeycomb grids, under thermal cyclic conditions to  $2500^\circ \text{C}$ , exhibited good mechanical stability but unsatisfactory fuel retention characteristics.
6. An unfueled tungsten cladding can be applied to the hexagonal channel walls to improve fuel retention at high temperatures, but more development work is needed.
7. In order to attain the program goals, additional development effort is necessary on all three processes.

Lewis Research Center,  
National Aeronautics and Space Administration,  
Cleveland, Ohio, April 5, 1967,  
122-28-01-01-22.

## APPENDIX - FUEL-PARTICLE-COATING PROBLEMS

As was discussed briefly in the text, one of the problem areas associated with radial variable fuel loadings was control of the thickness of the particle coating to fairly close tolerances so as to maintain fuel loading variations to within  $\pm 1$  volume percent  $\text{UO}_2$ . The following discussion of specific coating problems attempts to explain the difficulties of attaining close control of fuel loading tolerances.

This problem is pointed out in figure 18, in which calculated values for coating thickness are plotted against fuel loading for three substrate particle sizes. This figure shows possible variations in fuel loading of tungsten-coated  $\text{UO}_2$  particles for  $\text{UO}_2$  substrate particles in the range 30 to 60 microns. If the  $\text{UO}_2$  particle size is assumed to be 45 microns and the tungsten coating thickness to be 16 microns, the fuel loading is 20 volume percent. The tungsten coating thickness would have to be within 15.4 to 16.8 microns, in order to meet the fuel loading goal. However, with this thickness range but with  $\text{UO}_2$  particles in the range 30 to 60 microns, the fuel loading could vary from 11 volume percent at point A (in fig. 18) to 29.4 volume percent at point B. The average loading would be determined by the particle size distribution in the 30- to 60-micron range. If the particle size range were narrowed to 40 to 50 microns, then the range of fuel loading for the same coating variation would be narrowed to 16.5 to 23 volume percent.

In the coating process, the fuel loading is determined by weighing the substrate after coating to yield the average fuel loading of the batch. By this means, it is possible to minimize the effect of coating thickness, but this does not preclude the possibility of segregation of different sizes of coated particles during processing.

Thus, it appears that fuel loading variations must be controlled by narrowing the size range of the  $\text{UO}_2$  substrate particles. However, narrowing the usable size range would appreciably increase the cost of fuel (probably by a factor of 2 or 3 times the current cost) since the yield of usable particles from the spheroidization process would be extremely low. Therefore, compromises between fuel cost and the required fuel loading control might have to be made in producing tungsten- $\text{UO}_2$  fuel elements from tungsten-coated  $\text{UO}_2$  particles.



## REFERENCES

1. Krasner, Morton H.: A Reference Design for the Tungsten Water-Moderated Nuclear Rocket. Nuclear Rocket Technology Conference. NASA SP-123, 1966, pp. 159-173.
2. Lietzke, Armin F.: Water-Moderated Tungsten Nuclear Rocket Reactor Concept. NASA TM X-1044, 1965.
3. Gedwill, Michael A.; Sikora, Paul F.; and Caves, Robert M.: Fuel-Retention Properties of Tungsten-Uranium Dioxide Composites. NASA TM X-1059, 1965.
4. Goetsch, G. R.; Cover, P. W.; Gripshover, P. J.; Wilson, W. J.; and Boyer, C. B.: Fabrication of Tungsten- $\text{UO}_2$  Hexagonal-Celled Fuel-Element Configurations. Battelle Memorial Inst. (NASA CR-54796), Oct. 30, 1965.
5. Drumheller, K.; and Sump, K. R.: Fabrication of Tungsten-Uranium Dioxide Honeycomb Fuel Element Structures. Rep. No. BNWL-253 (NASA CR-54838), Battelle-Northwest, Sept. 1965.
6. Johnson, D. D.; Pettman, R. E.; and Jackson, D. E.: Fabrication of Tungsten- $\text{UO}_2$  Composites by a Powder Metallurgy Process. Rep. No. 3M-8439 (NASA CR-54424), Minnesota Mining and Mfg. Co., May 20, 1965.
7. Caves, Robert M.: High Temperature Performance of Vapor Deposition Tungsten Claddings on Tungsten-Uranium Dioxide Composites. NASA TM X-1449, 1967.
8. Hoppe, A. W.; and Lamartine, J. T.: Tungsten Cladding of Tungsten-Uranium Dioxide ( $\text{W-UO}_2$ ) Composites by Deposition from Tungsten Hexafluoride ( $\text{WF}_6$ ). Rep. No. WANL-PR(Z)-003 (NASA CR-54835), Westinghouse Electric Corp., 1965.
9. MacInnis, M. B.; and Schulze, H. O.: Tungsten Cladding of Tungsten-Uranium Dioxide Composites by Chloride Vapor Deposition. Rep. No. Syl-6335-FRI (NASA CR-54728), Sylvania. Electric Products, Inc., 1965.
10. Saunders, Neal T.; Gedwill, Michael A.; and Gluyas, Richard E.: Retention of Fuel in Tungsten-Uranium Dioxide Fuel Elements. Paper presented at the AIAA Joint Propulsion Specialists Conference, Colorado Springs, June 14-18, 1965. Also available as NASA TM X-52184.
11. Watson, Gordon K.; Caves, Robert M.; and Saunders, Neal T.: Preparation and Roll Compaction of Tungsten-Coated Uranium Dioxide Particles. NASA TM X-1448, 1967.

12. Spanner, J. C.; and Brown, R. L., Jr.: Development of Nondestructive Testing Methods for NASA Tungsten Water-Moderated Reactor Fuels. Vol. 1, Rep. No. BNWL-383 (NASA CR-72139), and Vol. 2, Rep. No. BNWL-384 (NASA CR-72140), Battelle-Northwest, 1967.
13. Buzzard, Robert J.; and Gill, Frank L.: High-Temperature Mechanical Properties of a Tungsten-Uranium Dioxide Composite. NASA TM X-1018, 1964.
14. Buzzard, Robert J.: Factors Affecting the Strength of Tungsten-Uranium Dioxide Composites. NASA TM X-1444, 1967.

TABLE I. - TYPE AND NUMBER OF  
SPECIMENS EVALUATED AT LEWIS

Fabrication process	Honeycomb grids	Plates
Hot isostatic compaction	8	10
Hot pneumatic impaction	12	12
Green-state forming and sintering (GSF)	4	10

TABLE II. - CHEMICAL ANALYSIS OF  
AS-FABRICATED SAMPLES

Fabrication process	Composition, weight percent			Halide impurities, ppm	
	Tungsten	Uranium dioxide	Yttrium oxide	Fluorine	Chlorine
Fuel loading, 10 volume percent (nominal)					
	93.54	5.91	0.55	(a)	(a)
Hot isotatic compaction	95.5	3.41	0.57	1600	----
Hot pneumatic impaction	93.8	4.14	.0635	----	1100
Green-state forming and sintering	94.4	4.68	.343	----	35
Fuel loading, 20 volume percent (nominal)					
	86.50	12.35	1.15	(a)	(a)
Hot isotatic compaction	89.5	8.88	1.00	5600	----
Hot pneumatic impaction	87.9	9.35	1.23	----	300
Green-state forming and sintering	89.4	10.05	.699	----	29
Fuel loading, 30 volume percent (nominal)					
	78.70	19.50	1.80	(a)	(a)
Hot isotatic compaction	84.0	12.66	1.44	600	----
Hot pneumatic impaction	81.1	15.72	1.94	----	200
Green-state forming and sintering	84.9	14.79	1.043	----	19

<sup>a</sup>Desired halide concentration less than 75 ppm total.

**CONFIDENTIAL**

TABLE III. - RESULTS OF ULTRASONIC AND  
EDDY-CURRENT ANALYSIS OF GRIDS

Type of grid		Number of grids inspected	Results of nondestructive tests	
Fabrication process	Configuration		Ultrasonic tests	Eddy-current tests
Hot isostatic compaction	Basic	3	Cracks in all three grids	Cracks in one grid; two grids sound
Hot pneumatic impaction	Alternate	3	Cracks in one grid; <sup>a</sup> two grids sound	Cracks in one grid; two grids sound
Green-state forming and sintering	Basic	1	Sound grid	Sound grid

<sup>a</sup>Same grid cracked in eddy-current test.

TABLE IV. - DENSITY OF TUNGSTEN - URANIUM DIOXIDE PLATES

Fabrication process	Fuel loading, vol. %	Density, g/cc		Percent of theoretical density	
		Theoretical <sup>a</sup>	Measured	Range	Average
Hot isostatic compaction	10	18.5	16.94	91.4	91.4
	20	17.6	16.65	94.7	94.7
	30	17.05	16.0 to 16.27	93.8 to 95.5	94.9
Hot pneumatic impaction	10	18.55	18.04 to 18.17	97.2 to 98.2	97.6
	20	17.5	16.67 to 17.02	95.5 to 97.2	96.2
	30	16.3	15.73 to 15.91	96.3 to 97.5	97.1
Green-state forming and sintering	10	18.4	17.70	96.2	96.2
	20	17.3	16.28	94.2	94.2
	30	16.7	15.33	91.8	91.8

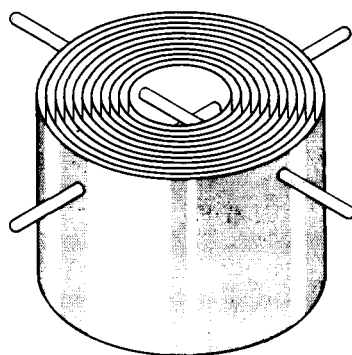
<sup>a</sup>Based on actual chemical analysis (table II).

**CONFIDENTIAL**

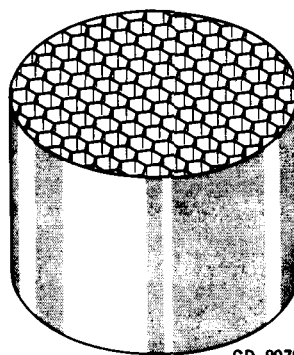
TABLE V. - ULTIMATE TENSILE STRENGTH OF  
PLATE SPECIMENS AT 2500° C

Fabrication process	Fuel loading, vol. %	Ultimate average tensile strength		Type of fracture
		psi	MN/m <sup>2</sup>	
Hot isostatic compaction	10	2365	16.3	Ductile
	20	2645	18.3	Ductile
	30	2410	16.7	Ductile
Hot pneumatic impaction	<sup>a</sup> 10	----	----	-----
	20	2190	15.1	Brittle
	30	2440	16.8	Brittle
Green-state forming and sintering	10	2990	20.6	Brittle
	20	2390	16.5	Brittle
	30	2170	15.0	Brittle

<sup>a</sup>Specimens broke in transit.



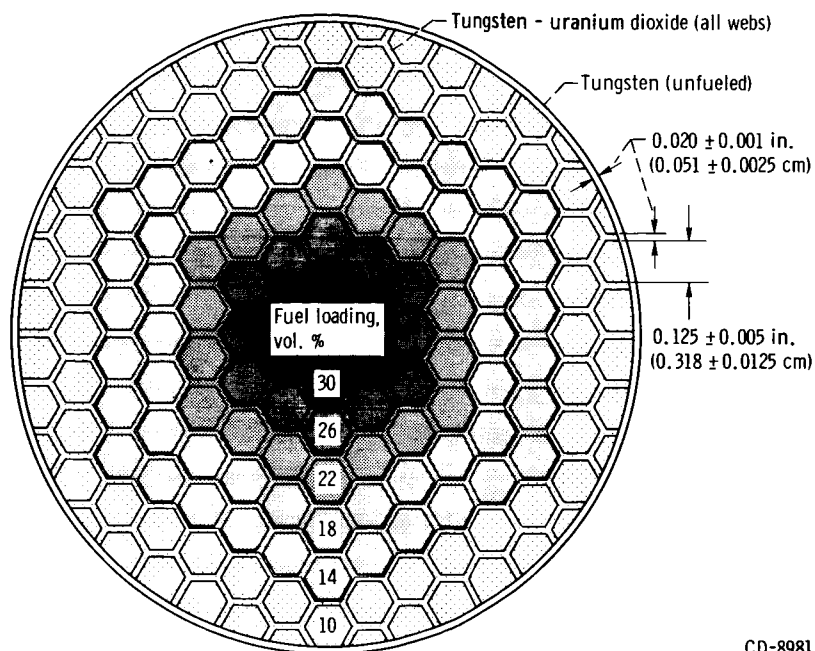
(a) Concentric cylinders.



CD-8978

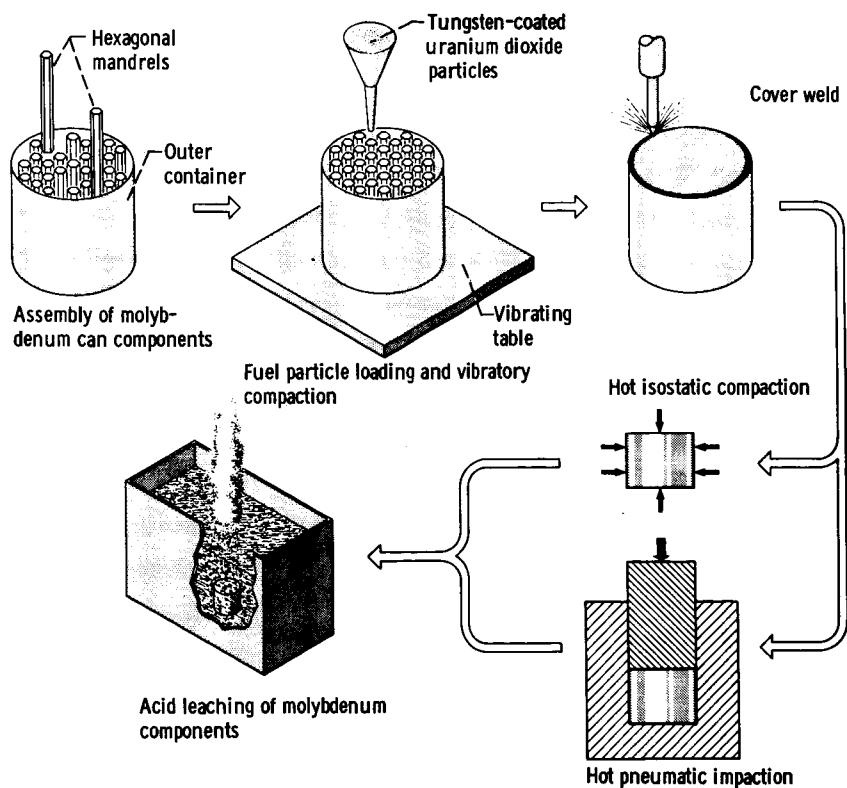
(b) Honeycomb array.

Figure 1. - Possible fuel element configurations for tungsten water-moderated reactor.  
Approximate dimensions, 2-inch (5 cm) outside diameter by 1.5 inches (3.7 cm) long.



CD-8981

Figure 2. - Cross section of basic hexagonal-celled honeycomb grid-configuration. Outer diameter,  $1.89 \pm 0.1$  inches ( $4.80 \pm 0.025$  cm); length,  $1.50 \pm 0.01$  inches ( $3.81 \pm 0.025$  cm).



CD-8980

Figure 3. - Can loading and processing steps for hot isostatic compaction and hot pneumatic impaction.

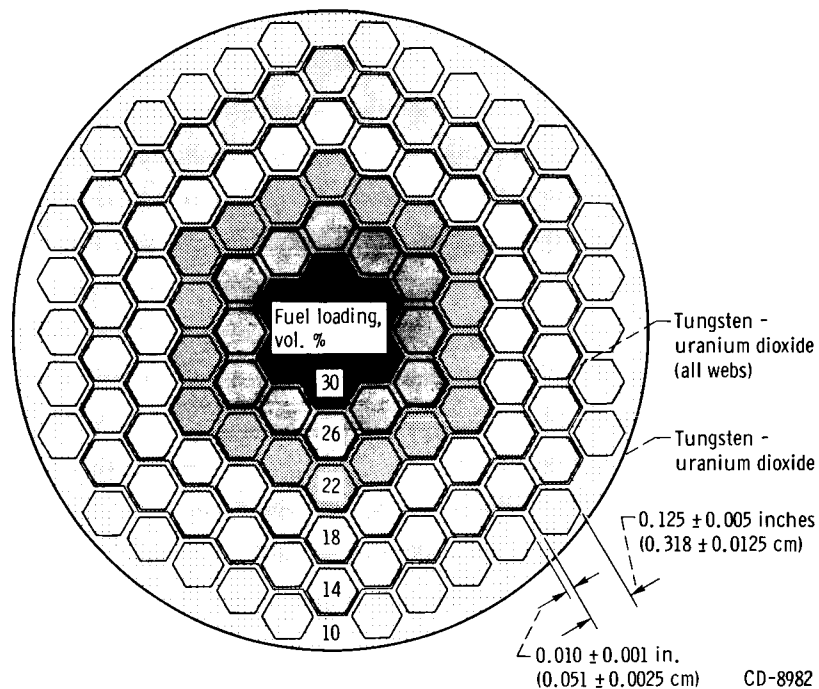


Figure 4. - Cross section of alternate hexagonal-celled honeycomb grid configuration. Outer diameter,  $1.77 \pm 0.01$  inches ( $4.50 \pm 0.035$  cm); length,  $1.50 \pm 0.01$  inches ( $3.81 \pm 0.025$  cm).

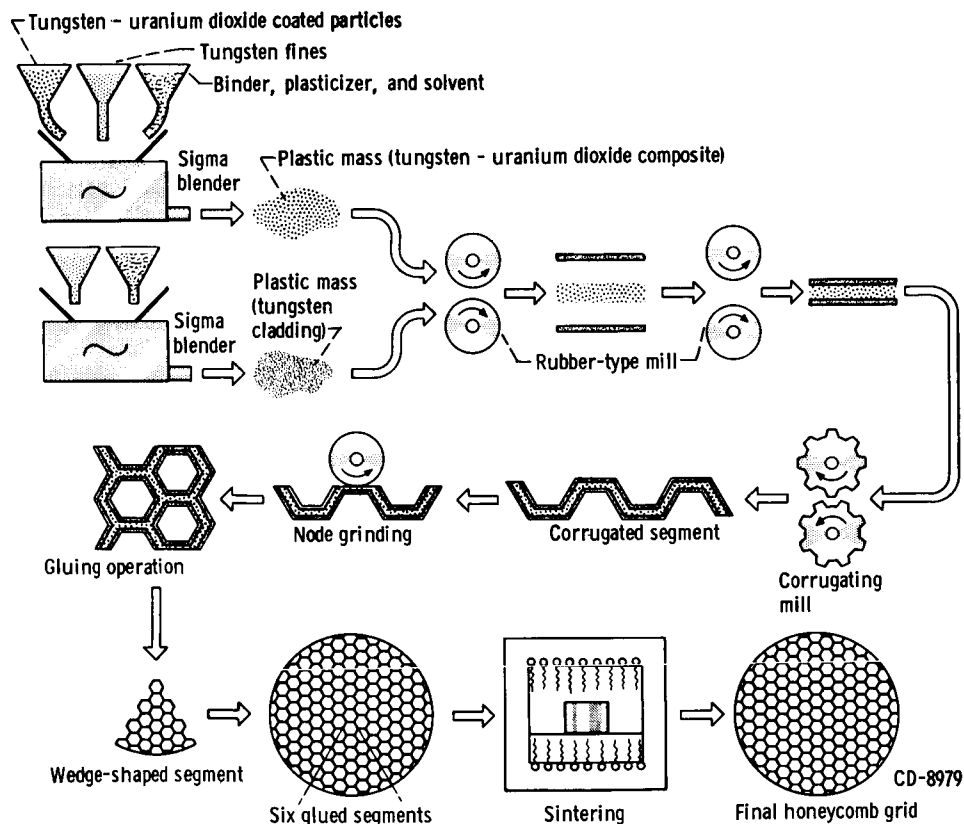
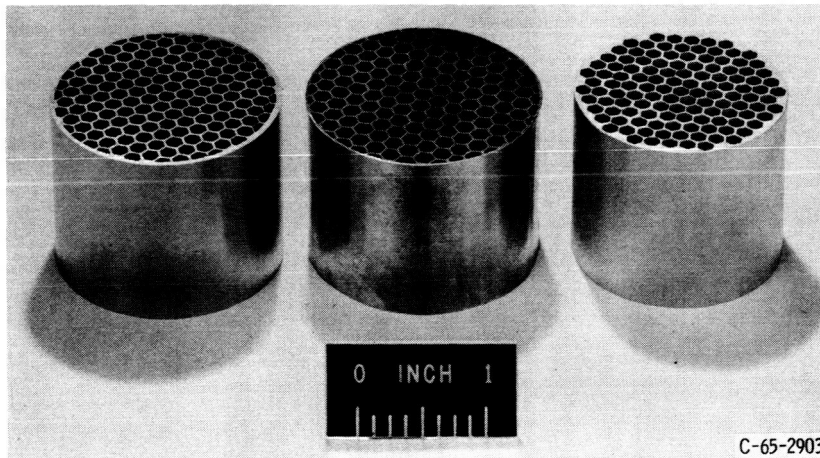


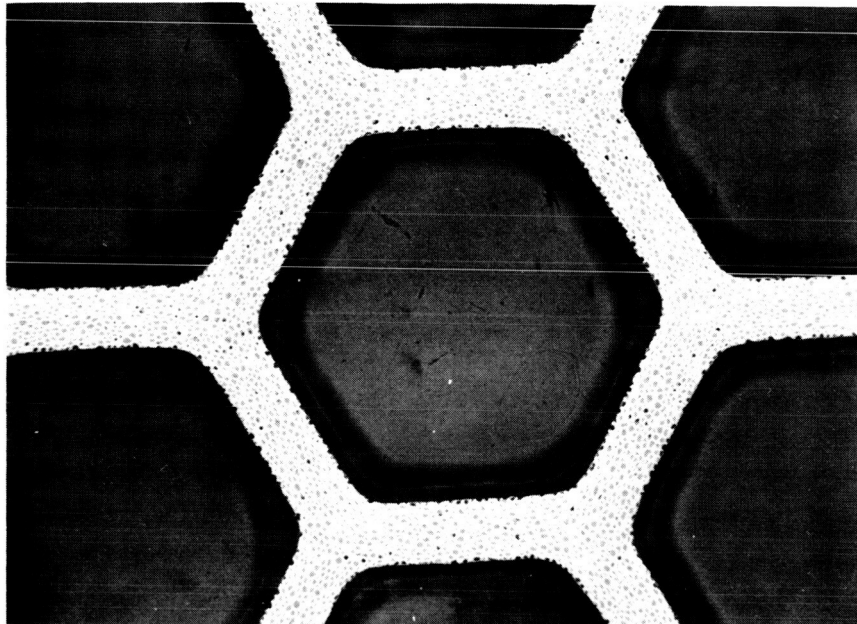
Figure 5. - Green-state forming and sintering process.





(a) Hot isostatic compaction. (b) Green-state forming and (c) Hot pneumatic impaction, sintering.

Figure 6. - Typical tungsten - uranium dioxide honeycomb structures fabricated by different processes.

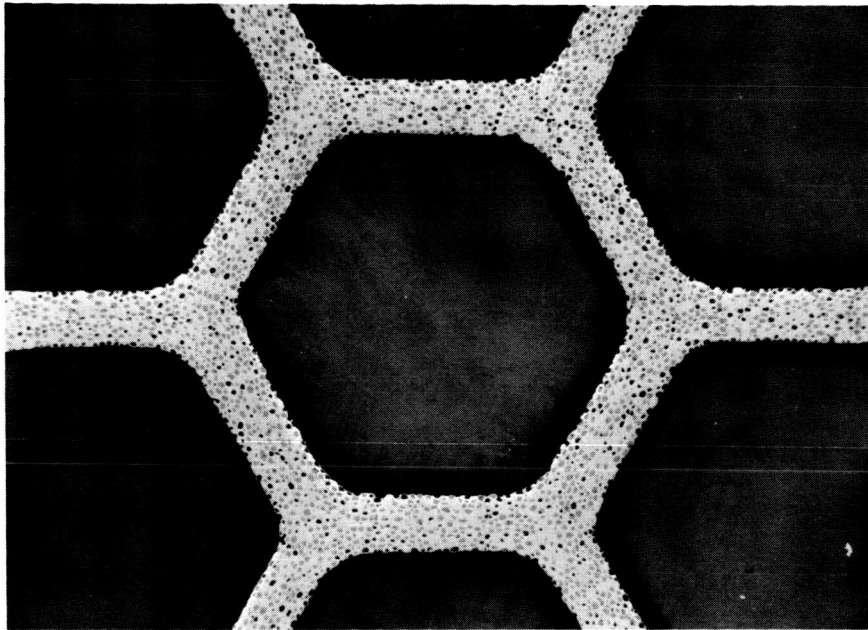


(a) Sound area.

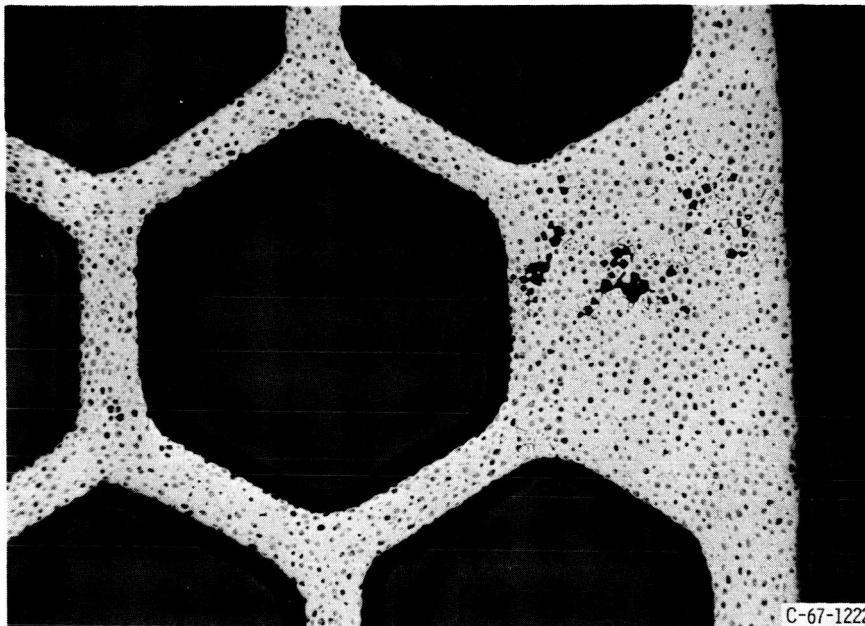


(b) Problem area.

Figure 7. - Typical hot isostatically compacted honeycomb grid. X15.



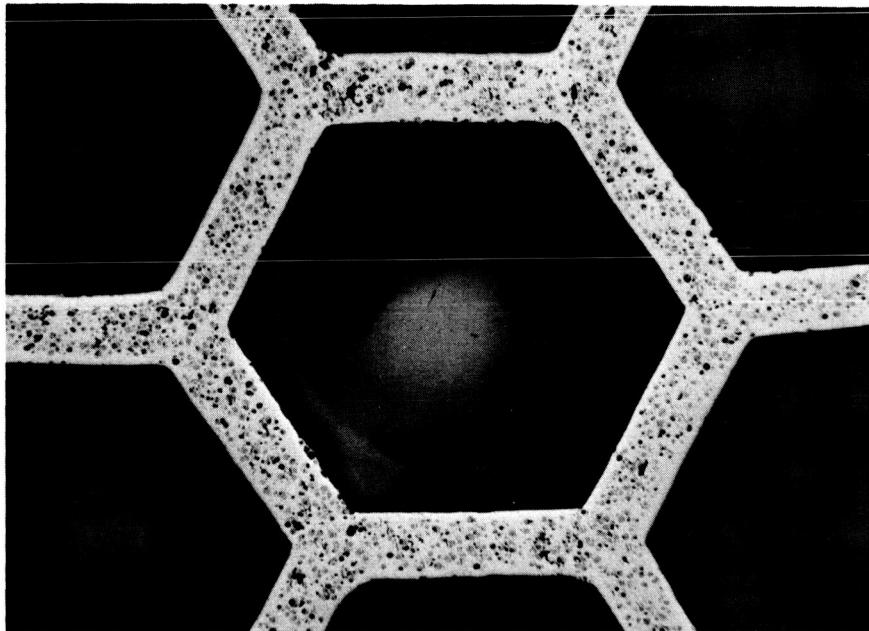
(a) Sound area.



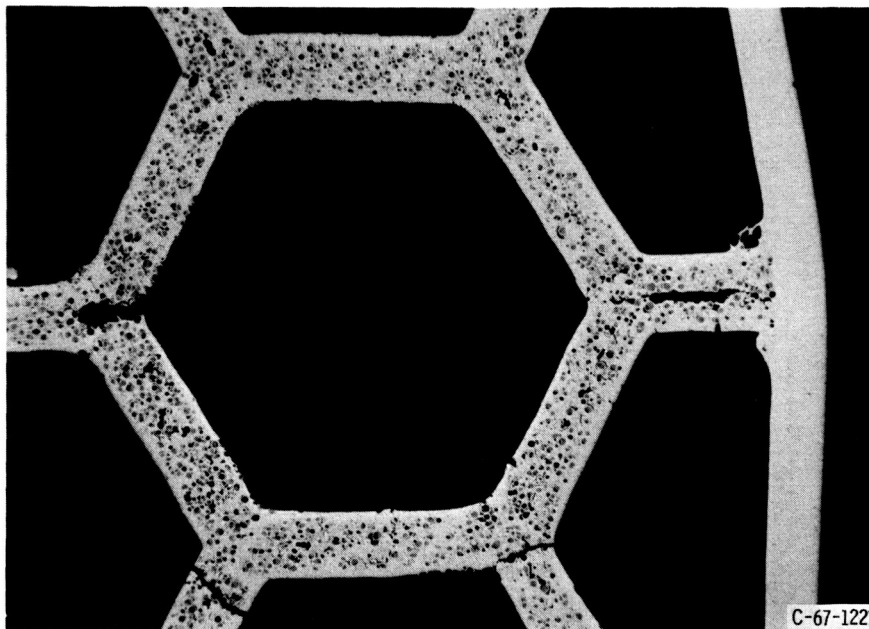
(b) Problem area.

Figure 8. - Typical hot pneumatically impacted honeycomb grid. X15.

~~CONFIDENTIAL~~



(a) Sound area.

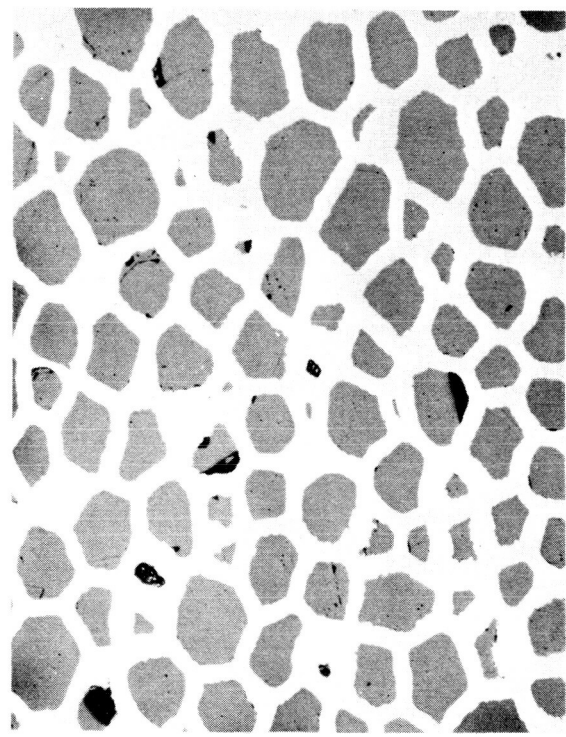


(b) Problem area.

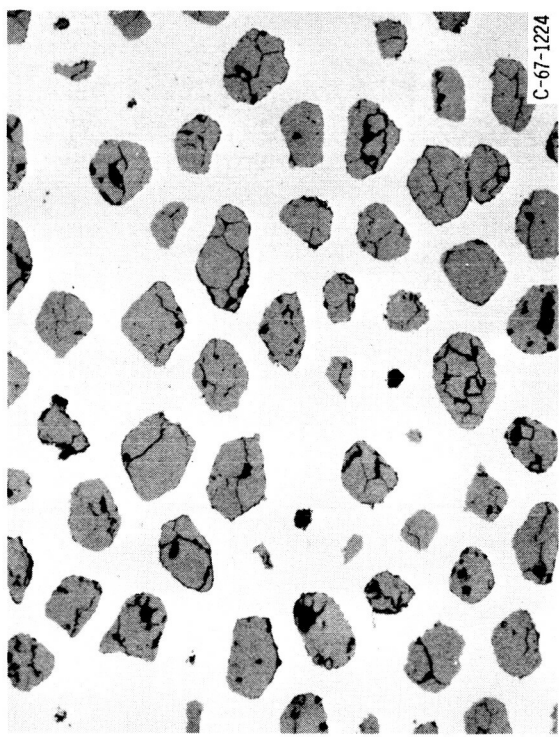
Figure 9. - Typical green-state formed and sintered honeycomb grid. X15.

~~CONFIDENTIAL~~

CONFIDENTIAL



(a) Hot isostatic compaction.



(b) Hot pneumatic impaction.

Figure 10. - Highly dense compacts of tungsten - uranium dioxide made by two processes using good starting materials. X150.

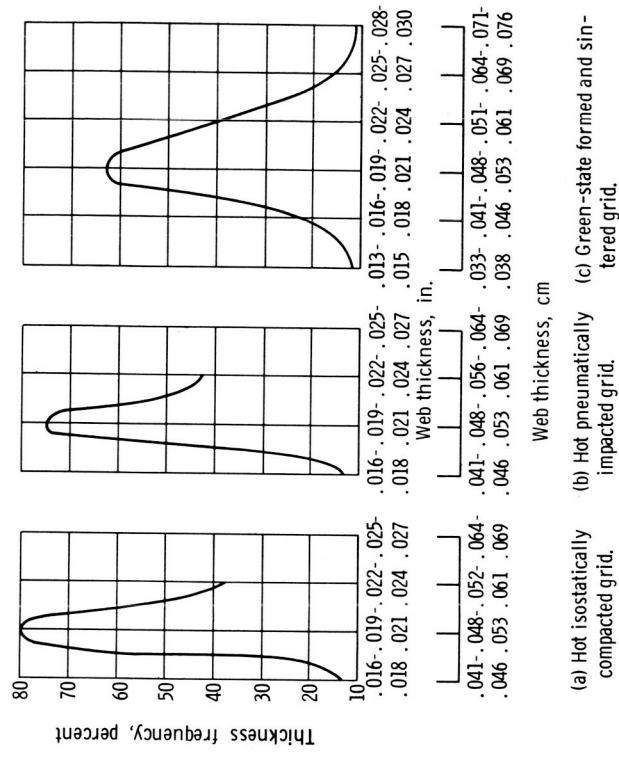


Figure 11. - Frequency distribution of web thickness for best grid from each fabrication process.

CONFIDENTIAL

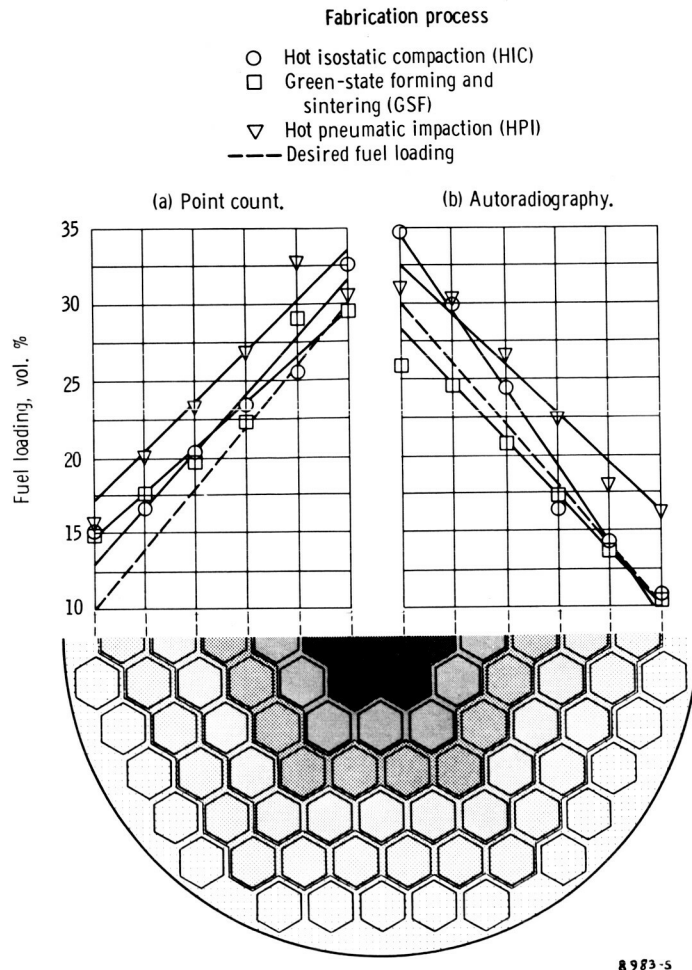


Figure 12. - Radial fuel loading as determined by autoradiography and point count of fuel particles.

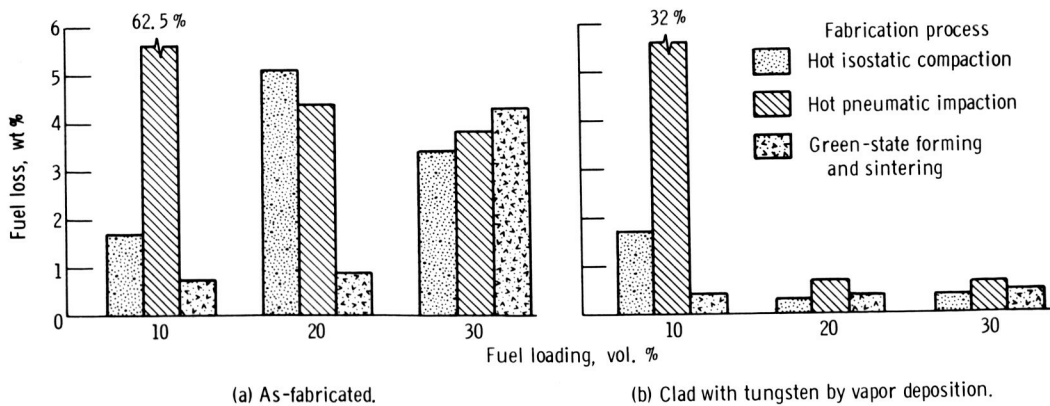
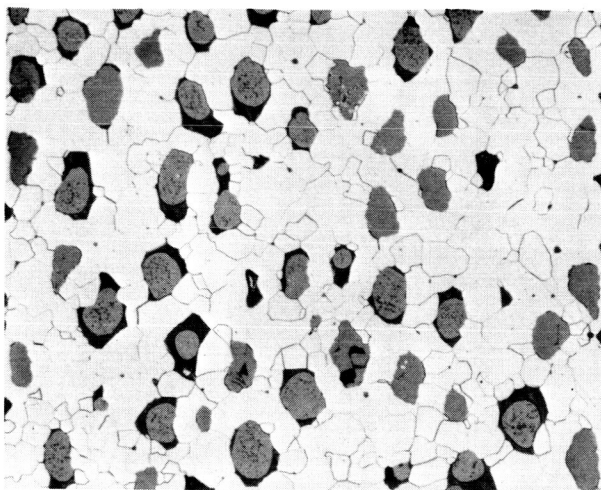
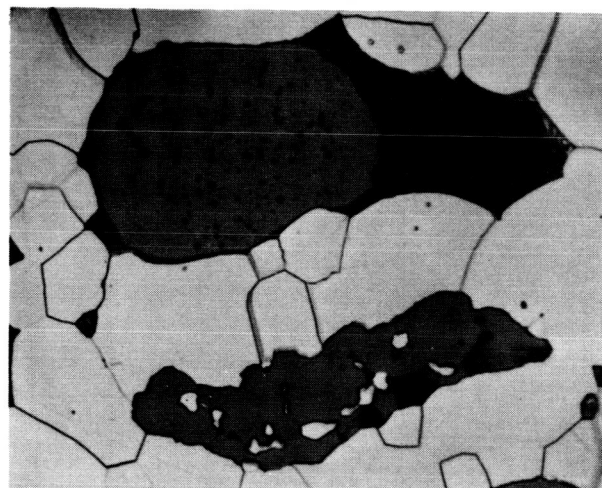


Figure 13. - Fuel loss from static thermal tests at 2500° C for 2 hours in hydrogen gas.

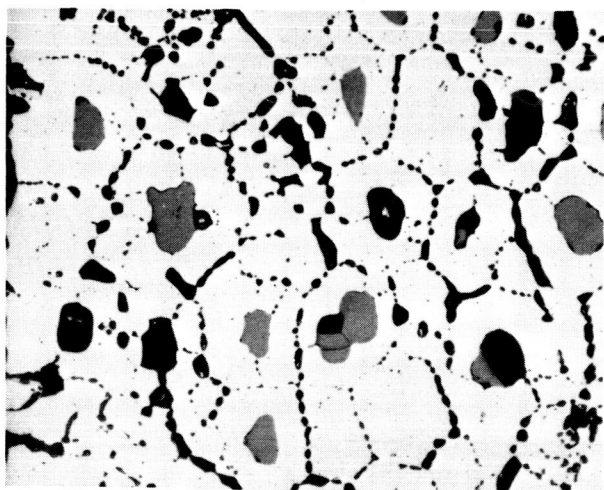




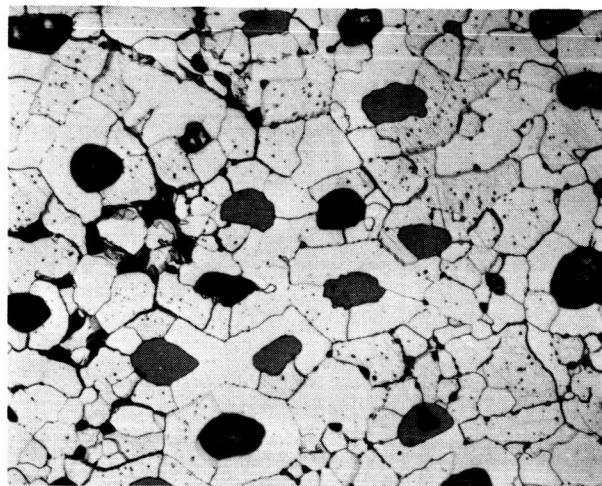
(a) Hot-isostatically compacted plate section. Etchant, Murakami's reagent. X150.



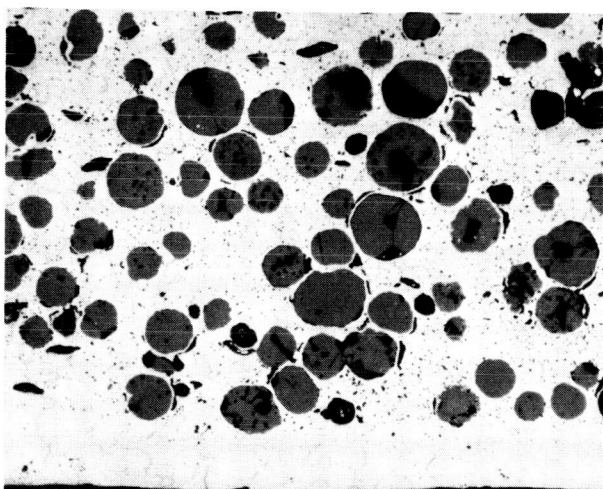
(b) Hot-isostatically compacted plate section. Etchant, Murakami's reagent. X750.



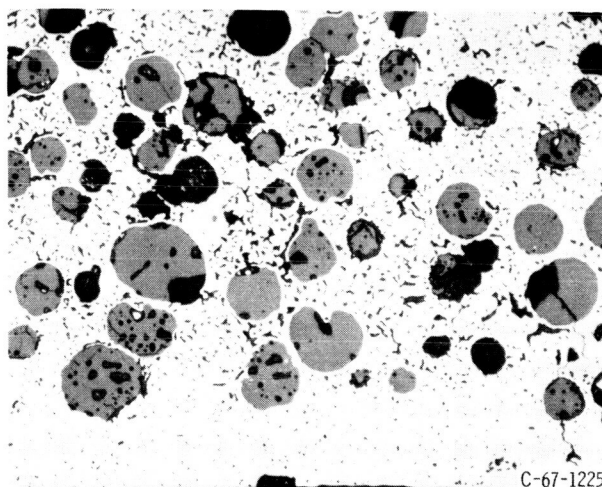
(c) Hot-pneumatically impacted plate section (after heat treating at 4500° F (2500° C)). Unetched, X150.



(d) Hot-pneumatically impacted grid section. Etchant, Murakami's reagent. X150.



(e) Green-state-formed plate section. Unetched. X150.



(f) Green-state-formed grid section. Unetched. X150.

Figure 14. - Typical effect of poor starting materials on microstructure of fabricated tungsten - uranium dioxide samples.

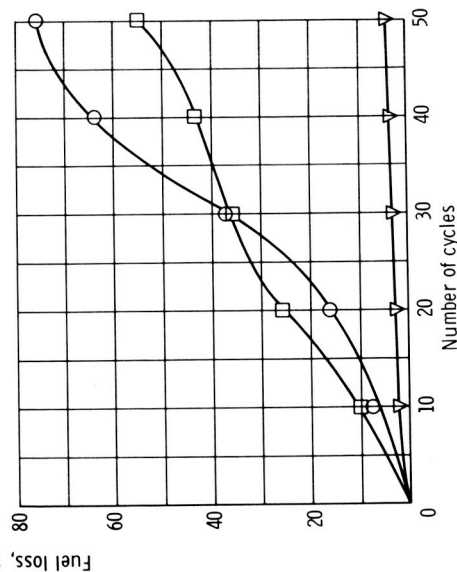
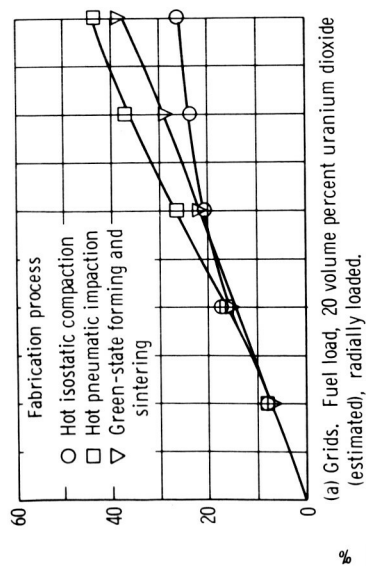


Figure 15. - Fuel loss from grid and plate after 10-minute thermal cycling to 2500°C in hydrogen gas.

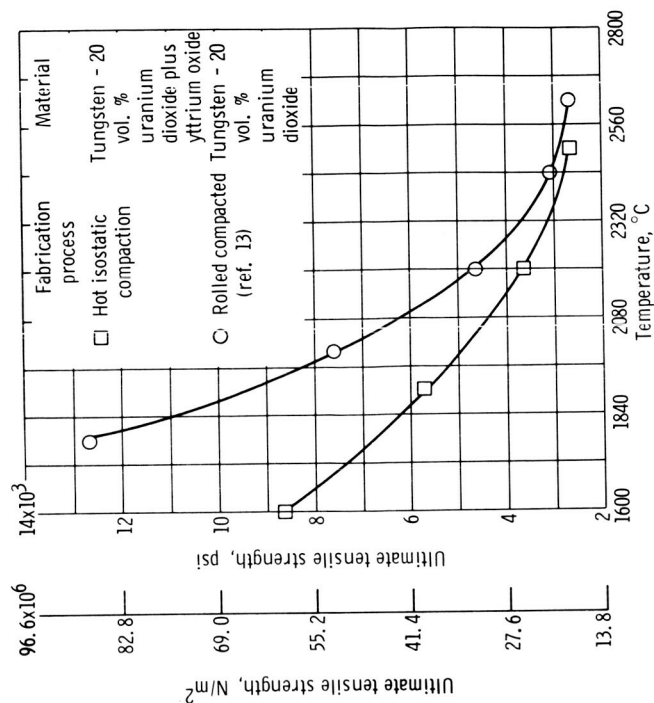
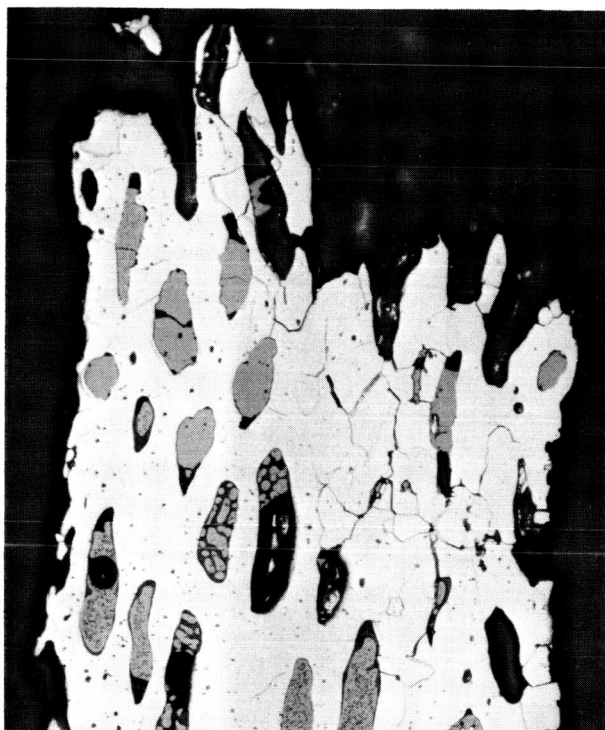
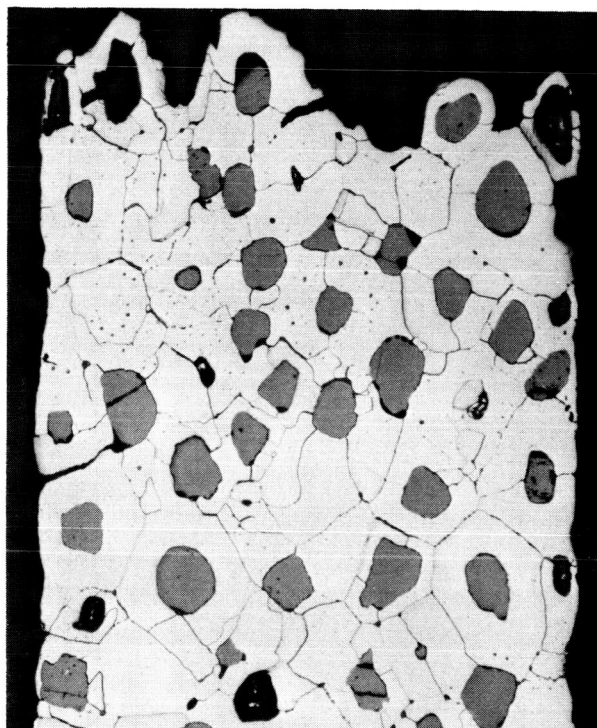


Figure 16. - Effect of temperature on ultimate tensile strength of tungsten - uranium dioxide composites fabricated from coated particles by different processes.

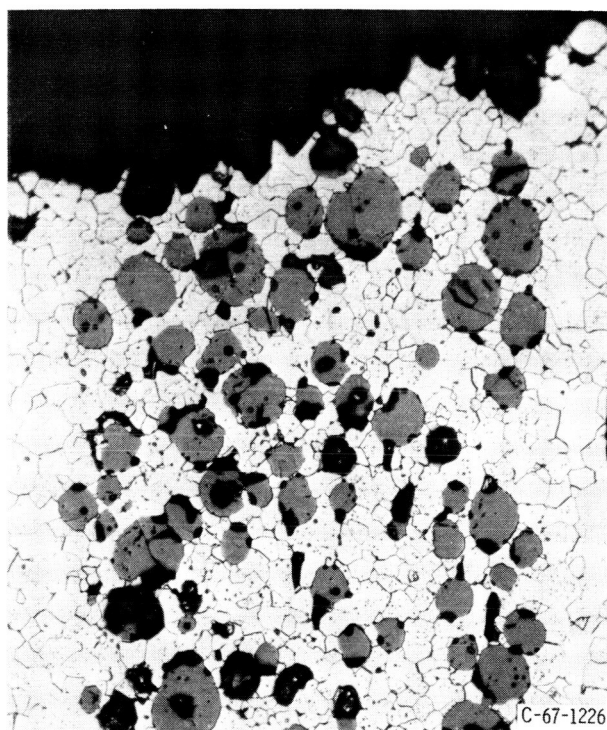




(a) Hot isostatic compacted, after tensile test.



(b) Hot pneumatic impacted, after tensile test.



(c) Green-state formed and sintered, after tensile test.

Figure 17. - Typical fracture zone after tensile testing at 2500° C. Etchant, Murakami's reagent. X150.

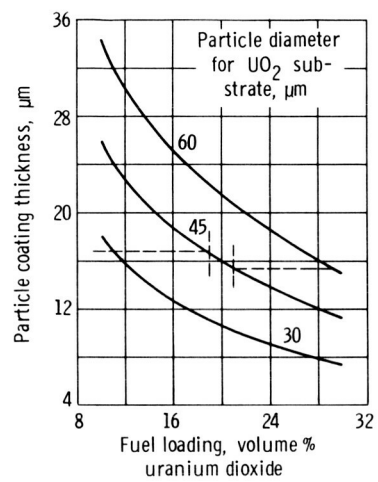


Figure 18. - Calculated effect of coating thickness on fuel loading of coated particles for substrate uranium dioxide ranging in diameter from 30 to 60 microns.

[REDACTED]

*"The aeronautical and space activities of the United States shall be conducted so as to contribute . . . to the expansion of human knowledge of phenomena in the atmosphere and space. The Administration shall provide for the widest practicable and appropriate dissemination of information concerning its activities and the results thereof."*

—NATIONAL AERONAUTICS AND SPACE ACT OF 1958

## NASA SCIENTIFIC AND TECHNICAL PUBLICATIONS

**TECHNICAL REPORTS:** Scientific and technical information considered important, complete, and a lasting contribution to existing knowledge.

**TECHNICAL NOTES:** Information less broad in scope but nevertheless of importance as a contribution to existing knowledge.

**TECHNICAL MEMORANDUMS:** Information receiving limited distribution because of preliminary data, security classification, or other reasons.

**CONTRACTOR REPORTS:** Scientific and technical information generated under a NASA contract or grant and considered an important contribution to existing knowledge.

**TECHNICAL TRANSLATIONS:** Information published in a foreign language considered to merit NASA distribution in English.

**SPECIAL PUBLICATIONS:** Information derived from or of value to NASA activities. Publications include conference proceedings, monographs, data compilations, handbooks, sourcebooks, and special bibliographies.

**TECHNOLOGY UTILIZATION PUBLICATIONS:** Information on technology used by NASA that may be of particular interest in commercial and other non-aerospace applications. Publications include Tech Briefs, Technology Utilization Reports and Notes, and Technology Surveys.

*Details on the availability of these publications may be obtained from:*

SCIENTIFIC AND TECHNICAL INFORMATION DIVISION  
NATIONAL AERONAUTICS AND SPACE ADMINISTRATION

Washington, D.C. 20546

[REDACTED]

1